ACS APPLIED MATERIALS & INTERFACES

www.acsami.org

Research Article

Ratiometric Dual Signal-Enhancing-Based Electrochemical Biosensor for Ultrasensitive Kanamycin Detection

Liang Tian, Yi Zhang, Liubo Wang, Qingjun Geng, Daxi Liu, Lili Duan, Yihong Wang,* and Jiansheng Cui*

Cite This: https://dx.doi.org/10.1021/acsami.0c15898

Read Online

ACCESS | Metrics & More | Article Recommendations | Supporting Information

ABSTRACT: Based on the signal amplification elements of planar VS_2/AuNPs nanocomposites and $CoFe_2O_4$ nanozyme, we herein developed an electrochemical biosensor for sensitive kanamycin (Kana) quantification. A ratiometric sensing platform was presented by incorporating VS_2/AuNPs nanocomposites as a support material with excellent conductivity and high specific surface area, as well as hairpin DNA (hDNA) with complementary hybridization of biotinylated Kana-aptamer. In addition, streptavidin-functionalized $CoFe_2O_4$ nanozyme with superior peroxidase-like catalytic activity were immobilized onto the aptasensor, hence the peroxidase-like catalytic reaction could yield amplified electrochemical signals. With the presence of Kana, the aptamer-biorecognition resulted in a quantitative decrease of nanozyme accumulation and an increase of methylene blue response. Under optimal conditions, the electrochemical signal ratio of the aptasensor revealed a linear relation along with the logarithmic concentration of Kana from 1 pM to 1 μM, with the limit of detection reaching to 0.5 pM. Moreover, this aptasensor exhibited excellent precision, as well as high repeatability, hence possessing potentials in real samples and for diverse targets detection by easy replacement of the matched aptamer.

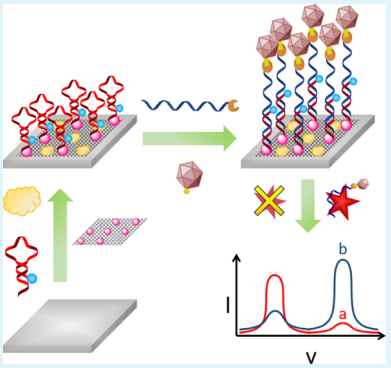

KEYWORDS: *electrochemical biosensor, ratiometric strategy, VS_2/AuNPs nanocomposites, $CoFe_2O_4$ nanozyme, kanamycin*

INTRODUCTION

Kanamycin (Kana) is a kind of aminoglycoside that is extensively used as an antibiotic for treating various bacterial infections; however, the abuse of Kana could ultimately lead to bioaccumulation in human body via the food chain and their existing residues may cause multiple serious human side effects, even antibiotic resistance.[1−3] As a result, a kind of simple, quick, and ultrasensitive strategy for the detection of antibiotic was desired.

Recently, various analytical technologies have been applied to sensitively detect the residues of antibiotic, including capillary electrophoresis, enzyme-linked immunosorbent assay (ELISA), fluorescence, and high-performance liquid chromatography (HPLC),[4−7] although most of them still have some limitation of tedious operation, high cost, and long operation time.[8] Therefore, one of the key aims for developing a detection method is to easily measure the residues in food or soil samples. Hence, many more rapid and cheap Kana measuring strategies have been emerging.

Currently, electrochemical analysis techniques have aroused great interests with the advantages of simple use, instrument miniaturization, low cost, and fast diagnostic and detection.[9] Compared with other Kana detection methods, electrochemical biosensors exhibit a dramatic alternative for Kana detection as they have the advantages of low detection limit, high sensitivity, good linear range, and good stability, which are suitable for the real-sample application.[10] DNA aptamer is a single-stranded deoxyribonucleic acid (DNA) sequence with many practical application advantages[11] that can be used as a target molecule recognition element for specifically recognizing the preselected target including metal ions, proteins, bacteria, virus, small organic molecules, pesticides, and antibiotics.[12] Thus, various DNA aptamers have been successfully applied to the high-specificity recognition of antibiotics.

Generally, two-dimensional (2D) nanomaterials are suitable for immobilization on the electrode surface of the electrochemical biosensor due to their unique physical and chemical features, including MoS_2, Mo_2C, and vanadium disulfide (VS_2).[13,14] VS_2, a typical transition-metal dichalcogenides (TMDs), presents a metallic electronic ground state; hence, triple-layered stacking 2D VS_2 nanosheets exhibit superior conductivity, large specific surface area, and superior mechanical properties.[15−18] Moreover, to improve the biocompatibility, gold nanoparticles (AuNPs) are applied in biosensors due to their superior biocompatibility, large surface

Received: September 3, 2020
Accepted: October 29, 2020

area, and remarkable conductivity.[19] Therefore, VS_2 nanosheets (NS) and AuNPs could be effectively combined to immobilize more probes and accelerate electron transfer easier.[20] Thus, the VS_2/AuNPs nanocomposites on the modified electrode will enhance the biosensor signal greatly by increasing the charge transfer rate and efficiently retaining the biomolecule activities.

Numerous signal amplification strategies including hybridization chain reaction (HCR), rolling circle amplification (RCA), and catalytic hairpin assembly (CHA) have been developed for biosensor components. However, the use of nuclease and enzymatic probe still has some disadvantages, such as sensitivity to sensing environment and requirement of optimal temperature.[21] Hence, the nonenzyme ratiometric dual signal-enhancing strategy has great potential for biosensing platform construction due to its short reaction time, wide linear range, high reliability, and improved sensitivity and selectivity.[22] To increase the sensitivity of aptasensor, a variety of natural enzymes possessing great catalytic efficiency as well as wonderful specificity have been used in signal amplification, however, they still have limitations that are susceptible to environmental impact.[23] Therefore, many more researchers have dedicated to develop nanomaterial-based enzyme (nanozyme) that has advantages of easy preparation, high activity to catalyze, and low cost.[24,25] Since then, various noble-metal-based nanomaterials, carbon-based nanomaterials, metal sulfide nanoparticles, metal-oxide-based nanoparticles, and hybrid nanoparticles have been discovered with oxidase, catalase, laccase, superoxide dismutase, and peroxidase mimicking activity.[26−28] Among these nanozyme, cobalt iron oxide ($CoFe_2O_4$), a bimetal hybrid oxide nanoparticle, is a practical way to enhance the signal amplification performance, which possess several virtues of high catalytic activity and remarkable stability.[29−31] Hence, the highly sensitive aptasensor could be achieved by using $CoFe_2O_4$ nanozyme as efficient signal amplification molecules.

Considering the above findings, we construct a ratiometric electrochemical aptasensor based on the VS_2/AuNPs nanocomposites as an electrode surface supporting material and methylene blue labeled hDNA (MB-hDNA) and $CoFe_2O_4$ nanozyme as signal amplification molecules for ultrasensitive and highly specific antibiotic detection. Herein, Kana was used as a model, and its high-efficiency amplification was driven by Kana-aptamer with the labeled $CoFe_2O_4$ nanozyme and MB-hDNA. Furthermore, due to the excellent charge transfer property of VS_2/AuNPs nanocomposites, the limit of detection of our aptasensor, which possesses good selectivity and reproducibility, has been remarkably improved as well. In addition, the aptasensor was also employed for detecting antibiotic residues in real milk samples for practical application verification.

EXPERIMENTAL SECTION

Reagents and Chemicals. NH_4VO_3, C_2H_5NS, $HAuCl_4$, $NaBH_4$, kanamycin sulfate, streptavidin (SA), bovine serum albumin (BSA), albumin, and casein were purchased from Sigma-Aldrich, while 3,3′,5,5′-tetramethylbenzidine (TMB), *N*-(3-dimethylaminopropyl)-*N*′-ethylcarbodiimide hydrochloride (EDC), *N*-hydroxysuccinimide (NHS), and hydrogen peroxide solution (30 wt %) were procured from Aladdin Reagent Company (Shanghai, China). All other reagents used in the study were of analytical grade unless otherwise stated. High-purity water was obtained from a Milli-Q water system (Millipore, Billerica, MA). Oligonucleotides used in this work were synthesized and purified by Sangon Biotech Co., Ltd. (Shanghai, China), and their base sequences are listed as follows: hDNA: 5′-SH-$(CH_2)_6$-TTT GTG GTC GGC TTA GCC TCA ACC CCC ATC TCC ACA AA-3′; MB-hDNA: 5′-SH-$(CH_2)_6$-TTT GTG GTC GGC TTA GCC TCA ACC CCC ATC TCC ACA AA-MB-3′; biotin-kanamycin aptamer: 5′-biotin-AGA TGG GGG TTG AGG CTA AGC CGA-3′.

Instrumentation. Electrochemical measurements were performed on a Gamry Reference 600 electrochemical workstation with a three-electrode system composed of a saturated calomel electrode as the reference electrode, a platinum wire as an auxiliary electrode, and a 3 mm diameter glassy carbon electrode (GCE) as the working electrode, respectively. The electrochemical techniques of cyclic voltammetry (CV), AC impedance (EIS), and differential pulse voltammetry (DPV) were carried out in a compound solution of 0.1 M KCl and 5 mM $[Fe(CN)_6]^{3-/4-}$, which served as a redox probe and supporting electrolyte. Also, transmission electron microscopy (TEM) images were obtained using FEI Tecnai G2 F20, while the powder X-ray diffraction (XRD) characterization was performed using X-ray diffraction (SmartLab, 3 KW, Japan) with Cu K radiation at room temperature. Additionally, ζ-potential analysis was measured on Zetasizer Nano ZS90. All measurements were carried out under a nitrogen atmosphere.

Preparation of VS_2 Nanosheets. VS_2 was synthesized by a hydrothermal reaction according to the previous report.[32] In brief, 2.0 mmol NH_4VO_3 and 20 mmol C_2H_5NS were dissolved in 30 mL of high-purity water containing 1.0 g of poly(vinylpyrrolidone) (PVP) and 2.0 mL of $NH_3{\cdot}H_2O$ and stirred for 1 h. Thereafter, the above mixture was placed in a 50 mL Teflon-lined stainless steel autoclave for heating reaction (180 °C, 20 h). Finally, the VS_2 nanosheets were obtained by washing the centrifugal separation product with high-purity water and ethanol several times and drying by freeze-drying.

Preparation of VS_2/AuNPs Composites. The VS_2/AuNPs composite was synthesized according to the previous protocol with some minor modifications.[33] To improve the dispersion, the VS_2 nanosheets were first functionalized with poly(ethylene glycol) (PEG 2000). Briefly, 40 mg of VS_2, 24 mg of PEG, and 30 mL of water were charged into a 50 mL beaker, stirred, and sonicated for 10 h. Subsequently, the precipitate was collected by centrifugation at 9000 rpm for 30 min and redispersed in water.

In preparing a VS_2/AuNPs composite, 4 mg of VS_2 nanosheets, 2 μL of 0.01 M $HAuCl_4$, and 2 mL of 0.01 M sodium citrate were added into 10 mL of ultrapure water, followed by the addition of 2 mL of 0.1 M 0−4 °C $NaBH_4$ solution with stirring for 30 min vigorously. Thereafter, the centrifugal separation product was washed with ultrapure water and ethanol and then dried by freeze-drying.

Synthesis of $CoFe_2O_4$ Nanozyme. The $CoFe_2O_4$ powders were prepared by a hydrothermal autoclave batch method.[34] Ten milliliters of precursor mixture containing 2.0 M $Fe(NO_3)_3{\cdot}9H_2O$, 1.0 M $Co(NO_3)_2{\cdot}6H_2O$, and 12.0 M NaOH was placed in a 15 mL Teflon-lined steel autoclave and heated at 200 °C for 1 h. Thereafter, the suspensions were centrifuged at 8000 rpm for 3 min, washed with ultrapure water three times, and dried by freeze-drying. Moreover, the obtained powders were then broken down in an agate mortar.

Functionalization of $CoFe_2O_4$ Nanozyme. First, sodium citrate was used to modify the surface of $CoFe_2O_4$ NPs. A 10 mL aqueous solution of 0.01 g of $CoFe_2O_4$ NPs and 0.2 g of sodium citrate were mixed and stirred for 1 h to obtain carboxy-protected $CoFe_2O_4$ NPs. Furthermore, to prepare the SA-modified $CoFe_2O_4$ NPs, EDC and NHS (1:1.2 mg mL^{-1}) were added into 1 mL of the above carboxy-terminated $CoFe_2O_4$ NP solution and incubated for 1 h.[35] After washing with phosphate-buffered saline (PBS) buffer, 50 μL of SA (1 mg mL^{-1}) was added and reacted overnight. Finally, the SA-conjugated $CoFe_2O_4$ nanozyme was washed and further blocked with BSA, as the final product was magnetically separated and suspended in the PBS buffer.

Fabrication of the Electrochemical Aptasensor. A bare GCE was first polished with 0.3 and 0.05 μm alumina slurry successively, followed by washing with ethanol and ultrapure water to obtain a clean and mirrorlike surface. Then, 5 μL of 2 mg mL^{-1} VS_2/AuNPs composite solution was dropped onto the surface of GCE and dried at

https://dx.doi.org/10.1021/acsami.0c15898
ACS Appl. Mater. Interfaces XXXX, XXX, XXX−XXX

Scheme 1. Schematic Illustration of the Preparation Process of the Aptasensor and the Electrochemical Detection Strategy of the Method

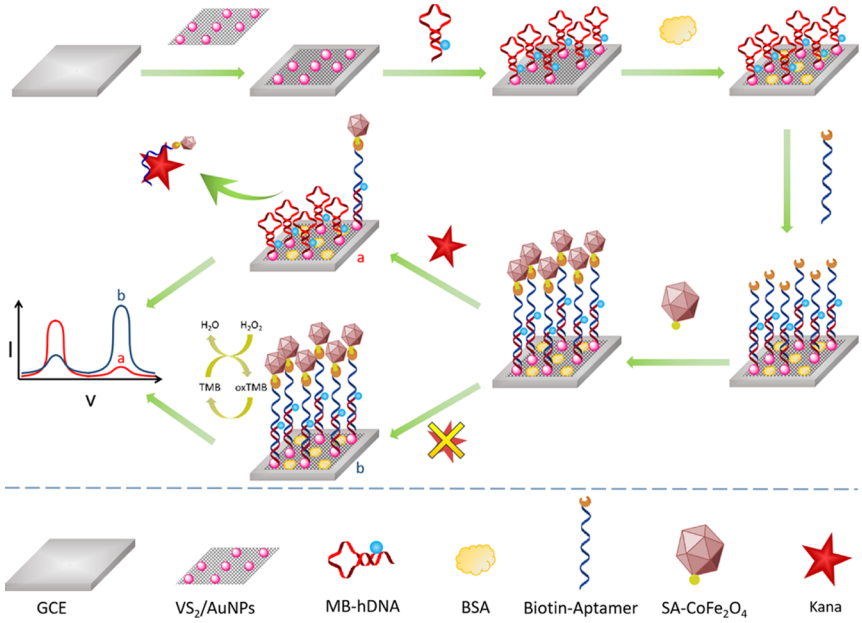

room temperature. Thereafter, 5 μL of 5 μM MB-hDNA was assembled on the surface of VS_2/AuNPs/GCE. After washing with 10 mM pH 7.0 PBS, a 5 μL drop of 1 mM BSA solution was cast onto the electrode surface to conduct a 60 min blocking reaction at room temperature. Furthermore, a 5 μL drop of 5 μM biotin-Kana-aptamer solution was further applied to its surface and then washed with PBS to remove the loosely adsorbed aptamer. Moreover, 5 μL of 1 mg mL^{-1} SA-modified $CoFe_2O_4$ nanozyme was dropped onto the resultant electrode. Finally, the obtained aptasensor was used to detect 5 μL of Kana in different concentrations in 0.01 M PBS with 0.1 mM of H_2O_2 and 0.2 mM of TMB. The illustration of the aptasensor preparation process and its electrochemical response for the quantitative analysis is depicted in Scheme 1.

Detection of Kana in Real Sample. To testify the reliability of real-sample detection, real milk samples without Kana were procured from a local supermarket, then diluted with PBS, and centrifuged for 10 min at 10 000 rpm for the separation of the deposit. Thereafter, the supernatant was filtered through a 0.22 μm sterile Millipore membrane, and the milk samples with Kana of multiple concentrations were obtained by the standard addition method to analyze the recovery rate.

RESULTS AND DISCUSSION

Principle and Feasibility of the Aptasensor. The working principle and detection feasibility of the electrochemical sensing platform for detecting Kana are represented in Scheme 1, with Kana selected as the model analyte. To enhance the electrochemical signal, the VS_2/AuNPs nanocomposites were applied as the electrode surface supporting material to remarkably accelerate the interface electron transfer, connect more biomolecules, and efficiently retain their activities. Then, VS_2/AuNPs/GCE was modified with sulfhydrylated MB-hDNA through the Au−S bond to hybridize the Kana-aptamer forming the double-strand structure. Subsequently, the obtained $CoFe_2O_4$ nanozyme can be used as a peroxidase mimic to catalyze and accelerate H_2O_2 into H_2O. In the absence of the target Kana, the $CoFe_2O_4$ nanozyme immobilized on the Kana-aptamer could also catalyze the substrate to produce a strong electronic signal within the environment of TMB and H_2O_2, and the opened hDNA keeps the MB signal molecules away from the electrode surface. However, when the target Kana exists, the electrochemical signal of the $CoFe_2O_4$ nanozyme decreased drastically and the MB signal increased, which could be ascribed to the dissociation of the $CoFe_2O_4$ nanozyme labeled aptamer from the electrode surface by Kana with higher affinity and the re-formed hDNA brings MB close to the electrode surface. Furthermore, the differential pulse voltammetry (DPV) verification is shown in Figure 1. The $CoFe_2O_4$

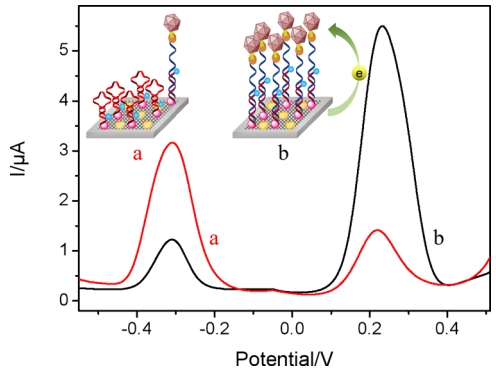

Figure 1. DPV curves of $CoFe_2O_4$ NPs/Kana-aptamer/MB-hDNA/VS_2/AuNPs/GCE in the presence (a) and absence (b) of 1 μM Kana target obtained in 0.01 M PBS (pH = 6.5).

nanozyme could undergo a peroxidase mimic catalysis in the absence of the Kana to provide a strong reduction current response of TMB at 0.23 V, while the reduction current response of MB at −0.31 V was weak (curve b). However, after the addition of the target Kana, the currents of TMB were significantly reduced and the MB response increased greatly (curve a), which demonstrated that the sensitivity of our electrochemical biosensor achieved great improvement by the proposed ratiometric strategy.

Characterization of the Nanomaterials. The XRD pattern confirmed that the prepared VS_2 nanosheets possessed

https://dx.doi.org/10.1021/acsami.0c15898
ACS Appl. Mater. Interfaces XXXX, XXX, XXX−XXX

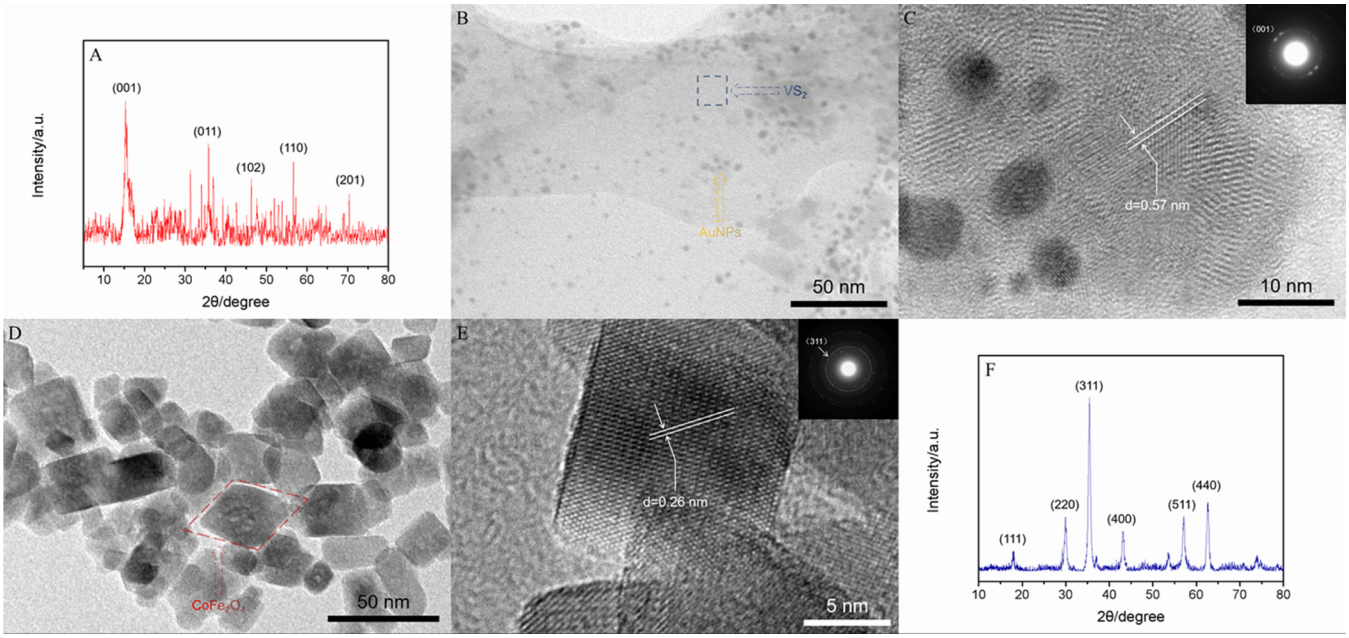

Figure 2. XRD pattern of VS_2 (A), TEM image of VS_2/AuNPs (B), and HRTEM image of VS_2/AuNPs (C) with SAED pattern (inset). TEM image of $CoFe_2O_4$ nanozyme (D), HRTEM image of $CoFe_2O_4$ nanozyme (E) with SAED pattern (inset), and XRD pattern of $CoFe_2O_4$ nanozyme (F).

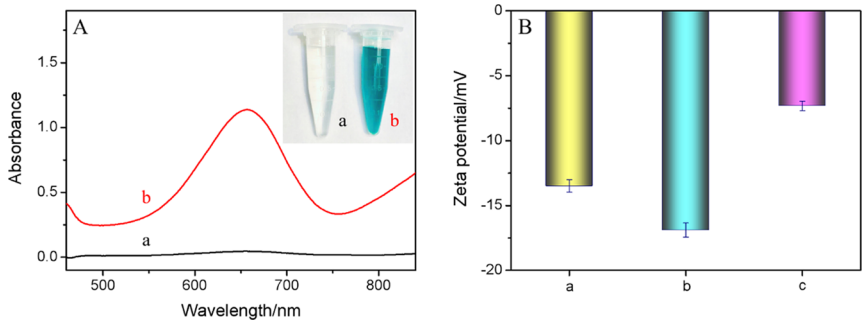

Figure 3. (A) UV−vis absorption spectra change of the TMB + H_2O_2 system (a) and TMB+H_2O_2 + $CoFe_2O_4$ nanozyme system (b) and the corresponding visual color changes (inset photo). (B) ζ-Potential of the naked $CoFe_2O_4$ nanozyme (a), carboxy-coated $CoFe_2O_4$ nanozyme (b), and streptavidin-coated $CoFe_2O_4$ nanozyme (c).

a trigonal structure, with the characteristic diffraction peaks corresponding to JCPDS Card No. 97-065-1361 (Figure 2A). Also, TEM was applied to characterize the morphologies and structure of the as-prepared nanomaterials. As shown in Figure 2B, a substantial number of dark dots were observed on the surface of the VS_2 nanosheet, indicating that AuNPs were concentrated on the VS_2 nanosheet with an average particle diameter of 3.7 nm (Figure S1). The high-resolution TEM (HRTEM) of the VS_2/AuNPs nanocomposites shown in Figure 2C suggested that the interplanar spacing of VS_2 nanosheets in the composite is estimated to be 0.57 nm, which corresponds to the (001) face, and its selected area electron diffraction (SAED) pattern is displayed in the inset. Furthermore, the energy-dispersive spectrometry (EDS) demonstrates that the elemental compositions of VS_2/AuNPs consist of V, S, and Au peaks, indicating that the VS_2/AuNPs nanocomposites were successfully synthesized (Figure S2). Additionally, CV and EIS characterizations of VS_2 NS and VS_2/AuNPs have been shown in Figure S3 where the VS_2/AuNPs present a higher current response in a CV than VS_2 NS (Figure S3A), as well as a lower Ret of 93 Ω in EIS than VS_2 NS of Ret = 190 Ω (Figure S3B). Hence, the addition of AuNPs to the VS_2 nanomaterial possess a positive effect on the electrode response due to their excellent electron transfer activity.[36] Besides, VS_2 NS can be delaminated to fewer layers after AuNPs are reduced on their surface, leading to an increased electron conductivity of VS_2/AuNPs. Moreover, the TEM image presented in Figure 2D shows that the $CoFe_2O_4$ nanozyme exhibited a cubic shape with an average diameter of 16 nm (Figure S4). As shown in Figure 2E, the HRTEM image of the $CoFe_2O_4$ nanozyme demonstrated that the interplanar spacing is 0.26 nm, corresponding to the (311) face as shown in the SAED pattern (inset). In addition, the XRD pattern (Figure 2F) indicates that the $CoFe_2O_4$ nanozyme is well-crystallized, with the characteristic diffraction peaks corresponding to JCPDS Card No. 03-0864. The EDS spectrum were carried out to investigate the elemental composition of the nanozyme, with Figure S5 showing the associated elements of Co, Fe, and O peaks that also confirmed the successful preparation of the $CoFe_2O_4$ nanozyme. Also, the peroxidase-like activity of the $CoFe_2O_4$ NPs was verified using TMB as a chromogenic agent. As shown in Figure 3A, the colorless TMB

https://dx.doi.org/10.1021/acsami.0c15898
ACS Appl. Mater. Interfaces XXXX, XXX, XXX−XXX

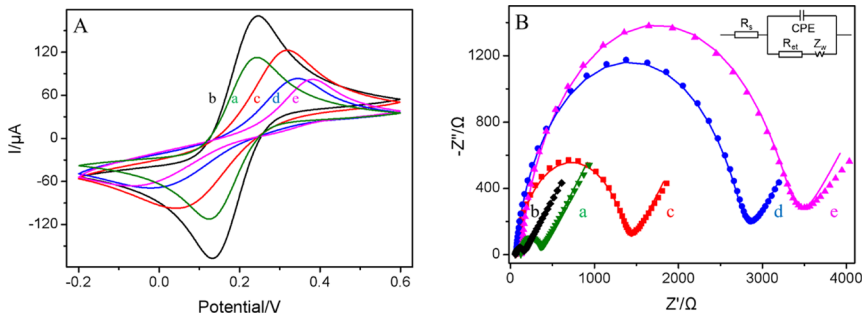

Figure 4. (A) Cyclic voltammograms and (B) Nyquist plots of electrochemical impedance spectra of bare GCE (a), VS_2/AuNPs/GCE (b), hDNA/VS_2/AuNPs/GCE (c), aptamer/hDNA/VS_2/AuNPs/GCE (d), and $CoFe_2O_4$ NPs/aptamer/hDNA/VS_2/AuNPs/GCE (d) in 5.0 mmol L^{-1} $[Fe(CN)_6]^{3-/4-}$ containing 0.1 mol L^{-1} KCl at 100 mV s^{-1}, and the frequency range is 100 mHz to 100 kHz with an amplitude of 5 mV (the inset is the equivalent circuit of the Nyquist plots).

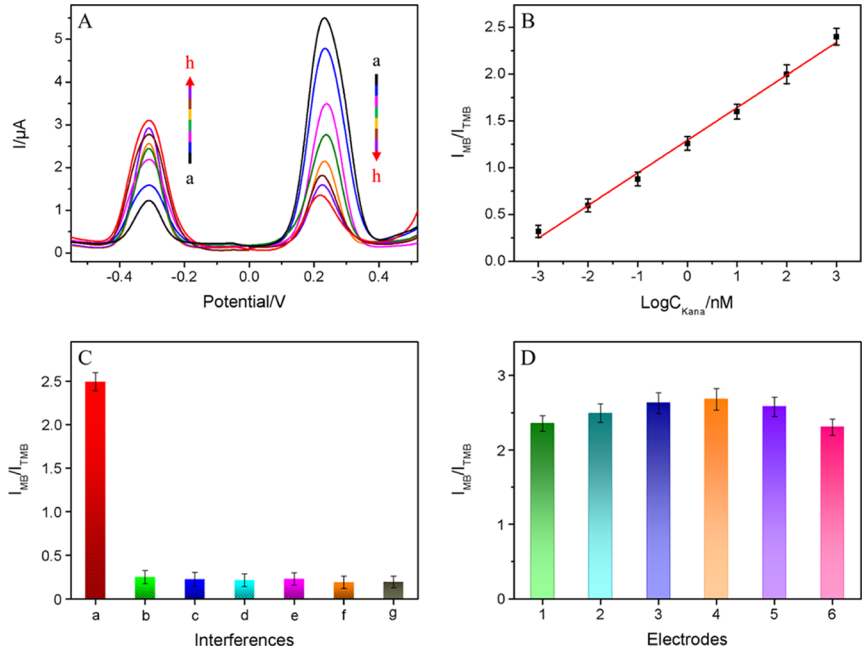

Figure 5. DPV response curves (A) of $CoFe_2O_4$ NPs/aptamer/MB-hDNA/VS_2/AuNPs/GCE fabricated ratiometric biosensor after capturing different concentrations of Kana from (a) to (h): 0 M, 1 pM, 10 pM, 100 pM, 1 nM, 10 nM, 100 nM, and 1 μM in 0.01 M PBS (pH = 6.5). (B) Calibration curve of I_{MB}/I_{TMB} vs logarithmic Kana concentration. (C) Specificity test of the proposed biosensor for kanamycin (a), tetracycline (b), norfloxacin (c), ampicillin (d), chloramphenicol (e), albumin (f), and casein (g) in 0.01 M PBS (pH = 6.5) and the concentrations were 1 μM. The I_{MB}/I_{TMB} of independently fabricated six biosensors (D). The concentrations were 1 μM. Error bars = RSD (n = 5).

(inset a) could be catalyzed into blue oxTMB (inset b) in the presence of $CoFe_2O_4$ NPs and H_2O_2 with an absorption peak of ultraviolet−visible (UV−vis) spectrum at 656 nm, indicating the superior peroxidase mimic activities of $CoFe_2O_4$ NPs. Besides, the signal amplification molecule of SA-functionalized $CoFe_2O_4$ nanozyme was characterized by ζ-potential. From Figure 3B, it could be seen that the ζ-potential of carboxy-coated $CoFe_2O_4$ nanozyme became lower than that of the naked electronegative $CoFe_2O_4$ nanozyme. However, after further conjugation of the positive SA, functionalization caused a dramatic change in the ζ-potential to become positive, which also increases, a confirmation that the $CoFe_2O_4$ nanozyme was successfully labeled with SA.

Characterization of Biosensor Fabrication. The fabrication procedures of the aptasensor were monitored by CV and EIS. As depicted in Figure 4A, CV measurement of VS_2/AuNPs nanocomposite-modified GCE (curve b) exhibited a stronger current response than bare GCE (curve a), suggesting the superior conductivity of the VS_2/AuNPs nanocomposites. Moreover, after the immobilization of hDNA (curve c) and the subsequent hybridization with Kana-aptamer (curve d), the current decreased continuously on account of the spatial blockage and negative charge density of DNA molecules near the electrode surface, indicating the successful immobilization of hDNA and Kana-aptamer. Finally, when $CoFe_2O_4$ NPs was bound, an aptamer-$CoFe_2O_4$ NPs layer was formed, leading to further decline of the peak current (curve e) as well as a more difficult electron transfer. The CV characterization revealed that VS_2/AuNPs nanocomposites and $CoFe_2O_4$ nanozyme could offer an enhanced electron transfer matrix for further catalysis pathways.

Measurements of EIS were also carried out to provide further information about the preparation of the biosensor, as shown in Figure 4B. The EIS spectra consisting of a semicircle section of high frequency and a straight section of low frequency, as well as the electromigration and diffusion control

https://dx.doi.org/10.1021/acsami.0c15898
ACS Appl. Mater. Interfaces XXXX, XXX, XXX−XXX

Table 1. Comparison of Different Biosensors for the Determination of Antibiotics

analytical technique	analyte	method of signal amplification	linear range	detection limit	refs
FRET	kanamycin	aptamer/donor (Cy3)-acceptor (Cy5)/PCA/CHA	1.0−80.0 nM	0.29 nM	38
eElectrochemical aptasensor	kanamycin	AuE/cDNA/Bio-apt/MB/Kana/AuNPs@HRP	2.0 pg mL^{-1} to 100 ng mL^{-1} (3 pM to 170 nM)	0.88 pg mL^{-1} (1.5 pM)	39
fluorometric	chloramphenicol	stirring bars/Y-shaped DNA probes/CAP/CHA/thioflavin T	0.05−10 nM	16 pM	40
evanescent wave aptasensor	aminoglycoside antibiotics	Cy3-aptamer/AMGA/GO/Anchor Aptamer	200 nM to 200 μM	26 nM	41
electrochemical	kanamycin and chloramphenicol	MB@Apt_1/Apt_2/M-NMOFs/Pb^{2+}/Cd^{2+}	0.002−100 nM	0.16 and 0.19 pM	42
electrochemical	ampicillin	GCE/AuNPs/aptamer/AuNPs-DNA/SSBP/ampicillin	1 pM to 5 nM	0.38 pM	43
electrochemical	kanamycin	GCE/VS_2/AuNPs/MB-hDNA/aptamer/$CoFe_2O_4$ NPs/kanamycin	1 pM to 1 μM	0.5 pM	this work

processes, were then analyzed by Gamry Echem Analyst software (inset of Figure 4B). Because of good conductivity, VS_2/AuNPs/GCE with 93 Ω in curve b displayed less resistance of electron transfer (Ret) than bare GCE with 217 Ω in curve a. Then, Ret was further increased to 1307 Ω (curve c) via blocking with hDNA. After treating with the aptamer, a significantly increased Ret of 2687 Ω was achieved in curve d, demonstrating the successful hybridization of hDNA and aptamer. Thereafter, aptamer/hDNA/VS_2/AuNPs/GCE was treated with $CoFe_2O_4$ NPs. As expected, the diameter of the semicircle remarkably increased to Ret of 3196 Ω in curve e with harder electronic transportation. All these EIS results implied that $CoFe_2O_4$ NPs/aptamer/hDNA/VS_2/AuNPs/GCE was successfully constructed, which were also in conformity with the aforementioned CV.

Optimization of Experimental Parameters. To improve the sensing performance, various parameters are required to be optimized, and these include incubation time, incubation temperature, and pH. From Figure S6A, it can be seen that the optimal incubation time of aptamer and Kana target were analyzed. With the increase in incubation time from 20 to 70 min, the reduction peak current of TMB decreased and reached a platform after 60 min, indicating a saturated capture process. Moreover, the optimum incubation temperatures of aptamer and Kana target were from 15 to 35 °C in Figure S6B, and the minimum value was obtained at 30 °C. Furthermore, the affect of pH of the measuring solution on the reduction current response of TMB is shown in Figure S6C. The current results decreased from pH 5.5 to 6.5 and increased from pH 6.5 to 7.5, indicating that this aptasensor could achieve an optimum signal response at pH 6.5 with superior affinity and structure of Kana-aptamer.

Analytical Performance of the Aptasensor. For the quantification of target Kana at different concentrations, the ratiometric sensing platform was evaluated by DPV under optimal conditions. As displayed in Figure 5A, the electrochemical TMB signal was found to gradually decrease and the MB signal increased with the increment of target Kana concentration, which represents that the content of Kana in the sample can be effectively revealed by the variation in the electrochemical signal. Besides, the plot of the electrochemical I_{MB}/I_{TMB} signal response vs the logarithm concentration of Kana showed a good linear correlation in the range from 1 pM to 1 μM, following the linear regression equation of I_{MB}/I_{TMB} = 0.348 log(C_{Kana}/nM) + 1.293 with a correlation coefficient of 0.994 (I is related to the peak current when the target exists) (Figure 5B). The limit of detection (LOD) was calculated as 0.5 pM with S/N = 3. By comparing the ratiometric dual signal-enhancing amplification to a single signal of MB-hDNA and a single signal of nanozyme, our ratiometric biosensor displayed a wilder linear range and a lower detection limit than only the MB-hDNA system (10 pM−100 nM, LOD = 3 pM; Figure S7A,B) and only the $CoFe_2O_4$ nanozyme-aptamer system (1 pM−1 nM, LOD = 0.8 pM; Figure S7C,D) respectively.[37] Furthermore, the sensitivity of the proposed ratiometric biosensor was equivalent to the previously reported works for Kana detection in Table 1, hence the present work exhibited simplicity and advantageous detection limit, which offers great potential in the real-sample application.

Specificity and Reproducibility of the Biosensor. Some other antibiotics of tetracycline, ampicillin, norfloxacin, chloramphenicol, and protein of albumin and casein were used for evaluating the specificity of the established aptasensor in the same experimental conditions. As shown in Figure 5C, the I_{MB}/I_{TMB} signal response of the Kana sample was much higher than those of other interfering substances, suggesting that the proposed ratiometric biosensor possesses better selectivity and specificity toward Kana. Besides, the corresponding voltammograms of the interference studies are shown in Figure S8.

Reproducibility is another important factor of the fabricated aptasensor, as examined at a Kana concentration of 1 μM. The relative standard deviation (RSDs) of five repeat experiments on an electrode for Kana was less than 3.16% (n = 5) as shown in Figure S9. Furthermore, six independent electrodes were prepared and used to detect Kana, and the RSDs were below 6.8% (Figure 5D). Thus, the designed ratiometric aptasensor-based assay in this study was precise, possessing a good reproducibility.

Real-Sample Analysis. The proposed aptasensor in the potential application for practical samples was investigated by detecting the Kana concentration in the real samples of milk. A concentration range from 100 pM to 1 μM was attained by employing the standard addition method. At last, the real milk sample tests of the aptasensor exhibited satisfactory practical application consequences with the recovery between 91.24 and 112.59%, as well as RSDs less than 5.26% (Table S1).

CONCLUSIONS

In summary, an ultrasensitive electrochemical ratiometric aptasensor was developed for Kana quantification using the VS_2/AuNPs nanocomposites as the sensing platform, MB-hDNA, and $CoFe_2O_4$ nanozyme for signal amplification. To the best of our knowledge, this is the first time that VS_2/AuNPs and $CoFe_2O_4$ NPs have been successfully applied in the field of antibiotic biosensing. The aptasensor revealed a linear current response ratio of I_{MB}/I_{TMB} with the Kana

https://dx.doi.org/10.1021/acsami.0c15898
ACS Appl. Mater. Interfaces XXXX, XXX, XXX−XXX

concentration in the range 1 pM to 1 μM and a LOD of 0.5 pM (S/N = 3). The high sensitivity could be attributed to the VS_2/AuNPs nanocomposites as electrode surface support material with excellent electron conductivity, as well as developing a ratiometric dual signal-enhancing strategy using MB and $CoFe_2O_4$ nanozyme with high catalytic activity as signal molecules for efficient and reliable signal amplification. Besides, the utilization of aptamer guaranteed detection selectivity with satisfactory recovery, making it possible to distinguish Kana from the other antibiotics. Furthermore, the established sensing strategy has excellent application potential for real milk samples and greatly reduces the complexity of the experiment, in addition to offering a very promising low-cost platform, which could further be extended to real-time detection of other antibiotics in the future.

■ ASSOCIATED CONTENT

Supporting Information

The Supporting Information is available free of charge at https://pubs.acs.org/doi/10.1021/acsami.0c15898.

Size distribution, EDS spectrum, cyclic voltammograms, Nyquist plots, optimization of the experimental parameters, DPV response curves, I_{MB}/I_{TMB} of the same fabricated biosensor, reproducibility assay, and real-sample detection (PDF)

■ AUTHOR INFORMATION

Corresponding Authors

Yihong Wang − *School of Chemistry and Chemical Engineering, Southeast University, Nanjing 211189, P. R. China*; Email: yihongwang@seu.edu.cn

Jiansheng Cui − *School of Environmental Science and Engineering, Hebei University of Science and Technology, Shijiazhuang, Hebei 050018, P. R. China*; Email: cui1603@163.com

Authors

Liang Tian − *School of Environmental Science and Engineering, Hebei University of Science and Technology, Shijiazhuang, Hebei 050018, P. R. China*; orcid.org/0000-0003-3036-414X

Yi Zhang − *School of Environmental Science and Engineering, Hebei University of Science and Technology, Shijiazhuang, Hebei 050018, P. R. China*

Liubo Wang − *School of Environmental Science and Engineering, Hebei University of Science and Technology, Shijiazhuang, Hebei 050018, P. R. China*

Qingjun Geng − *School of Environmental Science and Engineering, Hebei University of Science and Technology, Shijiazhuang, Hebei 050018, P. R. China*

Daxi Liu − *School of Environmental Science and Engineering, Hebei University of Science and Technology, Shijiazhuang, Hebei 050018, P. R. China*

Lili Duan − *School of Environmental Science and Engineering, Hebei University of Science and Technology, Shijiazhuang, Hebei 050018, P. R. China*

Complete contact information is available at: https://pubs.acs.org/10.1021/acsami.0c15898

Author Contributions

The manuscript was written through contributions of all authors. All authors have given approval to the final version of the manuscript.

Notes

The authors declare no competing financial interest.

■ ACKNOWLEDGMENTS

This research was financially supported by the National Natural Science Foundation of China (Nos. 21407040 and 81571812), the Natural Science Foundation of Hebei Province (No. 20543901D), and the Scientific Research Foundations for Introduced Talents of Hebei University of Science and Technology (No. 1181375).

■ REFERENCES

(1) Ye, Y.; Wu, T.; Jiang, X.; Cao, J.; Ling, X.; Mei, Q.; Chen, H.; Han, D.; Xu, J.; Shen, Y. Portable Smartphone-Based QDs for the Visual Onsite Monitoring of Fluoroquinolone Antibiotics in Actual Food and Environmental Samples. *ACS Appl. Mater. Interfaces* **2020**, *12*, 14552−14562.

(2) Majdinasab, M.; Mishra, R. K.; Tang, X. Q.; Marty, J. L. Detection of Antibiotics in Food: New Achievements in the Development of Biosensors. *TrAC, Trends Anal. Chem.* **2020**, *127*, No. 115883.

(3) He, X.; Han, H.; Liu, L.; Shi, W.; Lu, X.; Dong, J.; Yang, W.; et al. Self-Assembled Microgels for Sensitive and Low-Fouling Detection of Streptomycin in Complex Media. *ACS Appl. Mater. Interfaces* **2019**, *11*, 13676−13684.

(4) Nguyen, T. A. H.; Pham, T. N. M.; Le, T. B.; Le, D. C.; Tran, T. T. P.; Nguyen, T. Q. H.; Nguyen, T. K. T.; Hauser, P. C.; Mai, T. D. Cost-effective Capillary Electrophoresis with Contactless Conductivity Detection for Quality Control of Beta-lactam Antibiotics. *J. Chromatogr. A* **2019**, *1605*, No. 360356.

(5) Bajkacz, S.; Felis, E.; Kycia-Slocka, E.; Harnisz, M.; Korzeniewska, E. Development of a New SLE-SPE-HPLC-MS/MS Method for the Determination of Selected Antibiotics and their Transformation Products in Anthropogenically Altered Solid Environmental Matrices. *Sci. Total Environ.* **2020**, *726*, No. 138071.

(6) Xiong, Y.; Leng, Y. K.; Li, X. M.; Huang, X. L.; Xiong, Y. H. Emerging Strategies to Enhance the Sensitivity of Competitive ELISA for Detection of Chemical Contaminants in Food Samples. *TrAC, Trends Anal. Chem.* **2020**, *126*, No. 115861.

(7) Wang, Y. H.; Yao, L.; Ning, G.; Wu, Y. H.; Wu, S.; Mao, S. M.; Liu, G. Q. An Electrochemical Strategy for Tetracycline Detection Coupled Triple Helix Aptamer Probe with Catalyzed Hairpin Assembly Signal Amplification. *Biosens. Bioelectron.* **2019**, *143*, No. 111613.

(8) Wang, W.; Sang, Q. Q.; Yang, M.; Du, J.; Yang, L. B.; Jiang, X.; Han, X. X.; Zhao, B. Detection of Several Quinolone Antibiotic Residues in Water Based on Ag-TiO_2 SERS Strategy. *Sci. Total Environ.* **2020**, *702*, No. 134956.

(9) Zhang, R. F.; Wang, Y.; Qu, X. N.; Li, S. S.; Zhao, Y. H.; Liu, S.; Huang, J. D. Exonuclease III-powered DNA Walking Machine for Label-free and Ultrasensitive Electrochemical Sensing of Antibiotic. *Sens. Actuators, B* **2019**, *297*, No. 126771.

(10) Nishitani, S.; Sakata, T. Enhancement of Signal-to-Noise Ratio for Serotonin Detection with Well-Designed Nanofilter-Coated Potentiometric Electrochemical Biosensor. *ACS Appl. Mater. Interfaces* **2020**, *12*, 14761−14769.

(11) Taghdisi, S. M.; Danesh, N. M.; Nameghi, M. A.; Ramezani, M.; Alibolandi, M.; Hussanzadeh-Khayat, M.; Emrani, A. S.; Abnous, K. A Novel Electrochemical Aptasensor based on Nontarget-induced High Accumulation of Methylene Blue on the Surface of Electrode for Sensing of α-Synuclein Oligomer. *Biosens. Bioelectron.* **2019**, *123*, 14−18.

https://dx.doi.org/10.1021/acsami.0c15898
ACS Appl. Mater. Interfaces XXXX, XXX, XXX−XXX

(12) Li, J.; Yu, C. F.; Wu, Y. N.; Zhu, Y. J.; Xu, J. J.; Wang, Y.; Wang, H. T.; Guo, M. T.; Li, F. T. Novel Sensing Platform based on Gold Nanoparticle-aptamer and Fe-metal-organic Framework for Multiple Antibiotic Detection and Signal Amplification. *Environ. Int.* **2019**, *125*, 135−141.
(13) Samal, R.; Rout, C. S. Recent Developments on Emerging Properties, Growth Approaches, and Advanced Applications of Metallic 2D Layered Vanadium Dichalcogenides. *Adv. Mater. Interfaces* **2020**, *7*, No. 1901682.
(14) Sakthivel, R.; Kubendhiran, S.; Chen, S. M.; Kumar, J. V. Rational Design and Facile Synthesis of Binary Metal Sulfides VS_2-SnS_2 Hybrid with Functionalized Multiwalled Carbon Nanotube for the Selective Detection of Neurotransmitter Dopamine. *Anal. Chim. Acta* **2019**, *1071*, 98−108.
(15) Su, J. W.; Wang, M. S.; Li, Y.; Wang, F. K.; Chen, Q.; Luo, P.; Han, J. B.; Wang, S.; Li, H. Q.; Zhai, T. Y. Sub-millimeter-scale Monolayer p-type H-phase VS_2. *Adv. Funct. Mater.* **2020**, *30*, No. 2000240.
(16) Ji, Q. Q.; Li, C.; Wang, J. L.; Niu, J. J.; Gong, Y.; Zhang, Z. P.; Fang, Q. Y.; Zhang, Y.; Shi, J. P.; Liao, L.; Wu, X. S.; Gu, L.; Liu, Z. F.; Zhang, Y. F. Metallic Vanadium Disulfide Nanosheets as a Platform Material for Multifunctional Electrode Applications. *Nano Lett.* **2017**, *17*, 4908−4916.
(17) Li, L.; Li, Z. D.; Yoshimura, A.; Sun, C. L.; Wang, T. M.; Chen, Y. W.; Chen, Z. Z.; Littlejohn, A.; Xiang, Y.; Hundekar, P.; Bartolucci, S. F.; Shi, J.; Shi, S. F.; Meunier, V.; Wang, G. C.; Koratkar, N. Vanadium Disulfide Flakes with Nanolayered Titanium Disulfide Coating as Cathode Materials in Lithium-ion Batteries. *Nat. Commun.* **2019**, *10*, No. 1764.
(18) Zhang, Z. P.; Niu, J. J.; Yang, P. F.; Gong, Y.; Ji, Q. Q.; Shi, J. P.; Fang, Q. Y.; Jiang, S. L.; Li, H.; Zhou, X. B.; Gu, L.; Wu, X. S.; Zhang, Y. F. Van der waals Epitaxial Growth of 2D Metallic Vanadium Diselenide Aingle Crystals and their Extra-high Electrical Conductivity. *Adv. Mater.* **2017**, *29*, No. 1702359.
(19) Scanlon, M. D.; Smirnov, E.; Stockmann, T. J.; Peljo, P. Gold Nanofilms at Liquid-liquid Interfaces: An Emerging Platform for Redox Electrocatalysis, Nanoplasmonic Sensors, and Electrovariable Optics. *Chem. Rev.* **2018**, *118*, 3722−3751.
(20) Khosropour, H.; Rezaei, B.; Rezaei, P.; Ensafi, A. A. Ultrasensitive Voltammetric and Impedimetric Aptasensor for Diazinon Pesticide Detection by VS_2 Quantum Dots-graphene Nanoplatelets/carboxylated Multiwalled Carbon Nanotubes as a New Group Nanocomposite for Signal Enrichment. *Anal. Chim. Acta* **2020**, *1111*, 92−102.
(21) Chen, X.; Huang, J.; Zhang, S.; Mo, F.; Su, S.; Li, Y.; Fang, L. C.; Deng, J.; Huang, H.; Luo, Z. X.; Zheng, J. S. Electrochemical Biosensor for DNA Methylation Detection through Hybridization Chain-Amplified Reaction Coupled with a Tetrahedral DNA Nanostructure. *ACS Appl. Mater. Interfaces* **2019**, *11*, 3745−3752.
(22) Hu, R.; Zhang, X.; Chi, K. N.; Yang, T.; Yang, Y. H. Bifunctional MOFs-Based Ratiometric Electrochemical Sensor for Multiplex Heavy Metal Ions. *ACS Appl. Mater. Interfaces* **2020**, *12*, 30770−30778.
(23) He, Z. J.; Kang, T. F.; Lu, L. P.; Cheng, S. Y. An Electrochemiluminescence Aptamer Sensor for Chloramphenicol Based on GO-QDs Nanocomposites and Enzyme-linked Aptamers. *J. Electroanal. Chem.* **2020**, *860*, No. 113870.
(24) Wang, H.; Wan, K. W.; Shi, X. H. Recent Advances in Nanozyme Research. *Adv. Mater.* **2019**, *31*, No. 1805368.
(25) Chen, Z. W.; Wang, Z. Z.; Ren, J. S.; Qu, X. G. Enzyme Mimicry for Combating Bacteria and Biofilms. *Acc. Chem. Res.* **2018**, *51*, 789−799.
(26) Mu, X. Y.; Wang, J. Y.; Li, Y. H.; Xu, F. J.; Long, W.; Ouyang, L. F.; Liu, H. L.; Jing, Y. Q.; Wang, J. Y.; Dai, H. T.; Liu, Q.; Sun, Y. M.; Liu, C. L.; Zhang, X. D. Redox Trimetallic Nanozyme with Neutral Environment Preference for Brain Injury. *ACS Nano* **2019**, *13*, 1870−1884.
(27) Li, L. J.; Zhang, J.; Zhang, M.; Rowell, N.; Zhang, C. C.; Wang, S. L.; Lu, J.; Fan, H. S.; Huang, W.; Chen, X. Q.; Yu, K. Fragmentation of Magic-Size Cluster Precursor Compounds into Ultrasmall CdS Quantum Dots with Enhanced Particle Yield at Low Temperatures. *Angew. Chem., Int. Ed.* **2020**, *59*, 12013−12021.
(28) Zhang, H.; Luan, C. R.; Gao, D.; Zhang, M.; Rowell, N.; Willis, M.; Chen, M.; Zeng, J. R.; Fan, H. S.; Huang, W.; Chen, X. Q.; Yu, K. Room-Temperature Formation Pathway for CdTeSe Alloy Magic-Size Clusters. *Angew. Chem., Int. Ed.* **2020**, *59*, 16943−16952.
(29) Zhu, W. D.; Li, M. X.; Chen, S. H.; Wang, C.; Lu, X. F. Interfacial engineering regulating the peroxidase-like property of ternary composite nanofibers and their sensing applications. *Appl. Surf. Sci.* **2019**, *491*, 138−146.
(30) Zhou, B. H.; Rinehart, J. D. A Size Threshold for Enhanced Magnetoresistance in Colloidally Prepared $CoFe_2O_4$ Nanoparticle Solids. *ACS Cent. Sci.* **2018**, *4*, 1222−1227.
(31) Li, F.; Chang, Q.; Li, N.; Xue, C. R.; Liu, H. T.; Yang, J. L.; Hu, S. L.; Wang, H. Q. Carbon Dots-stabilized Cu_4O_3 for a Multi-responsive Nanozyme with Exceptionally High Activity. *Chem. Eng. J.* **2020**, *394*, No. 125045.
(32) Meng, Y.; Zhao, Y. Y.; Wang, D. S.; Yang, D.; Gao, Y.; Lian, R. Q.; Chen, G.; Wei, Y. J. Fast Li^+ Diffusion in Interlayer-expanded Vanadium Disulfide Nanosheets for Li^+/Mg^{2+} Hybrid-ion Batteries. *J. Mater. Chem. A* **2018**, *6*, 5782−5788.
(33) Liu, X. Q.; Liu, P. P.; Tang, Y. F.; Yang, L. W.; Li, L. L.; Qi, Z. C.; Li, D. L.; Wong, D. K. Y. A Photoelectrochemical Aptasensor Based on a 3D Flower-like TiO_2-MoS_2-gold Nanoparticle Heterostructure for Detection of Kanamycin. *Biosens. Bioelectron.* **2018**, *112*, 193−201.
(34) Andersen, H. L.; Saura-Múzquiz, M.; Granados-Miralles, C.; Canevet, E.; Lock, N.; Christensen, M. Crystalline and Magnetic Structure-property Relationship in Spinel Ferrite Nanoparticles. *Nanoscale* **2018**, *10*, 14902−14914.
(35) Wu, L.; Xiao, X. Y.; Chen, K.; Yin, W. M.; Li, Q.; Wang, P.; Lu, Z. C.; Ma, J.; Han, H. Y. Ultrasensitive SERS Detection of Bacillus Thuringiensis Special Gene Based on Au@Ag NRs and Magnetic Beads. *Biosens. Bioelectron.* **2017**, *92*, 321−327.
(36) Zhang, H. X.; Wang, Z. H.; Wang, F.; Zhang, Y. M.; Wang, H. Y.; Liu, Y. In Situ Formation of Gold Nanoparticles Decorated Ti_3C_2 MXenes Nanoprobe for Highly Sensitive Electrogenerated Chemiluminescence Detection of Exosomes and Their Surface Proteins. *Anal. Chem.* **2020**, *92*, 5546−5553.
(37) Sun, H. B.; Kong, J. M.; Wang, Q. W.; Liu, Q. R.; Zhang, X. J. Dual Signal Amplification by eATRP and DNA-Templated Silver Nanoparticles for Ultrasensitive Electrochemical Detection of Nucleic Acids. *ACS Appl. Mater. Interfaces* **2019**, *11*, 27568−27573.
(38) Deng, J. K.; Liu, Y. Q.; Lin, X. D.; Lyu, Y. L.; Qian, P. C.; Wang, S. A Ratiometric Fluorescent Biosensor Based on Cascaded Amplification Strategy for Ultrasensitive Detection of Kanamycin. *Sens. Actuators, B* **2018**, *273*, 1495−1500.
(39) Chen, Z. C.; Lai, G. S.; Liu, S.; Yu, A. M. Ultrasensitive Electrochemical Aptasensing of Kanamycin Antibiotic by Enzymatic Signal Amplification with a Horseradish Peroxidase-functionalized Gold Nanoprobe. *Sens. Actuators, B* **2018**, *273*, 1762−1767.
(40) Hong, F.; Lin, X. T.; Wu, Y. X.; Dong, Y. R.; Cao, Y. T.; Hu, F. T.; Gan, N. Enzyme-free Fluorometric Assay for Chloramphenicol Based on Double Stirring Bar-assisted Dual Signal Amplification. *Microchim. Acta* **2019**, *186*, No. 150.
(41) Tang, Y. F.; Gu, C. M.; Wang, C.; Song, B. D.; Zhou, X. H.; Lou, X. H.; He, M. Evanescent Wave Aptasensor for Continuous and Online Aminoglycoside Antibiotics Detection Based on Target Binding Facilitated Fluorescence Quenching. *Biosens. Bioelectron.* **2018**, *102*, 646−651.
(42) Chen, M.; Gan, N.; Zhou, Y.; Li, T. H.; Xu, Q.; Cao, Y. T.; Chen, Y. J. A Novel Aptamer-metal Ions-nanoscale MOF Based Electrochemical Biocodes for Multiple Antibiotics Detection and Signal Amplification. *Sens. Actuators, B* **2017**, *242*, 1201−1209.
(43) Wang, J.; Ma, K.; Yin, H. S.; Zhou, Y. L.; Ai, S. Y. Aptamer Based Voltammetric Determination of Ampicillin Using a Single-stranded DNA Binding Protein and DNA Functionalized Gold Nanoparticles. *Microchim. Acta* **2018**, *185*, No. 68.

https://dx.doi.org/10.1021/acsami.0c15898
ACS Appl. Mater. Interfaces XXXX, XXX, XXX−XXX